e-Navi

Available online at http://www.e-navigation.kr/
e-Navigation Journal

Original article

Research on drag reduction of container ship's polygonal curved fairing based on CFD

Yefu Duan[a], Haihua Lin[b*], Chengmeng Sun[c]

[a] School of Naval Architecture and Port Engineering, Shandong Jiaotong University, Weihai 264209, China, 962694287@qq.com

[b*] School of Naval Architecture and Port Engineering, Shandong Jiaotong University, Weihai 264209, China, 7216219@qq.com, Corresponding Author

[c] School of Naval Architecture and Port Engineering, Shandong Jiaotong University, Weihai 264209, China, scmeng717@163.com

Abstract

In the context of the global shipping industry's transition towards high efficiency and low carbon emissions, energy conservation and drag reduction for ships have become core research directions in marine engineering. Container ships, as the backbone of international trade, experience a significant increase in wind resistance under extreme wind conditions of level 8 and above, which affects their navigation efficiency, energy consumption, and safety. Optimizing wind resistance is crucial for enhancing ship performance and reducing carbon emissions.

The fairing can reduce the air resistance of ships by optimizing the flow field and suppressing vortex flows, presenting broad application prospects. However, existing research has primarily focused on conventional wind conditions, and further analysis is needed under extreme wind conditions. Given the typicality and harmfulness of level 8 winds, this paper takes large container ships as the research object. Based on Computational Fluid Dynamics (CFD) numerical simulations, by establishing key structural models, optimizing computational domains and grids, and selecting the Realizable k-ε turbulence model and Volume of Fluid (VOF) multiphase flow model, this study investigates the drag reduction effect of polygonal curved fairings under level 8 wind speeds. It analyzes parameters such as drag coefficient and flow field distribution, reveals the flow field regulation mechanism, and provides theoretical support and data reference for the optimal design and engineering application of fairings.

Keywords: Ship resistance; Fairing; CFD

https://doi.org/10.52820/j.enavi.2025.25.035

1. Introduction

International trade serves as the core bond connecting economies of various countries. Shipping, with its advantages such as large volume and low cost, accounts for 80% of global cargo transportation. However, its carbon emissions have a significant impact on the ecological environment. Coupled with the increasingly stringent international regulations on ship energy efficiency, the research and application of ship drag reduction technology have become increasingly crucial.

The wind resistance of conventional ships accounts for 2% to 4% of the total resistance, with limited impact. However, due to the dense stacking of containers on the deck, container ships have an increased windward area, making the impact of wind resistance more prominent. Reducing wind resistance has become an important direction for drag reduction in container ships. The fairing reduces wind resistance by optimizing the streamlined shape of the hull, offering advantages of low cost and high cost-effectiveness.

The quantitative research and structural optimization of the drag reduction effect of fairing not only promote the iterative upgrading of ship drag reduction technology, but also have important practical significance for reducing carbon emissions in the shipping industry and protecting the global ecological environment.

2. Ship resistance analysis

2.1 Total ship resistance

Ship resistance refers to the counteracting force generated by the interaction between water and air when a ship navigates in water (Wang et al., 2026). This force not only hinders the ship's forward movement but also directly affects its navigation efficiency. Ship resistance (Sanz et al., 2026; He, 2020) can be classified into various types based on its causes, fluid medium, and other factors. The focus of this article is on the total resistance of the ship (i.e., the combined effect of all resistances) and the wind resistance above the water surface of the ship.

In practical calculations, due to factors such as scale model testing, directly expressing ship resistance may introduce deviations. Therefore, to more scientifically and accurately characterize ship resistance, non-dimensional numbers or coefficients (such as ship resistance coefficients) are commonly used as measurement indicators.

In this article, the total resistance coefficient of a ship is defined as:

$$C_T = \frac{R_T}{0.5\rho V^2 S} \tag{1}$$

In the formula, R_T represents the total resistance of the ship, N; ρ is the density of water, kg/m³ ; V is the ship speed, m/s; and S is the wet surface area of the hull, m² .

2.2 Wind resistance of ships

During the navigation of ships, wind can exert adverse effects on ships, (Forrest & Owen, 2010; Grlj et al., 2023; Viola, 2009) primarily manifesting as drag and capsizing forces. The wind force can be decomposed into two components: a longitudinal force along the length of the ship and a lateral force along the width of the ship (Wu, Song, Zhang, Wang, & Gu, 2025)Given that the focus of this paper is on ship drag, only the longitudinal component of wind force is considered. To facilitate quantitative analysis, a dimensionless longitudinal wind force coefficient is used to describe the impact of wind on the longitudinal motion of the ship. Its specific definition is as follows:

$$C_{\mathrm{w}} = \frac{F_x}{0.5\rho_a V_a^{\,2} A_T} \tag{2}$$

In the formula: F_x represents the longitudinal wind force along the ship's length, N; ρ_a represents air density, kg/m³ ; V_a represents the longitudinal absolute wind speed, m/s; A_T represents the longitudinal wind-exposed area, m² .

Based on drag analysis, a numerical calculation model will be constructed and validated in the following text to ensure the accuracy of drag reduction effect evaluation.

3. Numerical calculation method

3.1 Governing equations

Reynolds decomposed the instantaneous variables in the instantaneous control equations into two parts: the mean and the fluctuating components. For velocity, it is expressed as:

$$u_i = \overline{u_i} + u_i' \tag{3}$$

In the formula, $\overline{u_i}$ represents the average velocity, m/s; u' represents the pulsating velocity, m/s.

Similarly, for other scalars, we have:

$$\phi = \overline{\phi} + \phi' \tag{4}$$

In the formula: ϕ represents a scalar.

Substituting the above expression into the instantaneous continuity equation and momentum conservation equation, we obtain the Reynolds-averaged equation:

$$\frac{\partial \rho}{\partial t} + \frac{\partial (\rho \overline{u_i})}{\partial x_i} = 0 \tag{5}$$

$$\begin{gathered} \frac{\partial (\rho \overline{u_i})}{\partial t} + \frac{\partial (\rho \overline{u_i}\,\overline{u_j})}{\partial x_j} = \\ \frac{\partial}{\partial x_j}\left[\mu\left(\frac{\partial \overline{u_i}}{\partial x_j} + \frac{\partial \overline{u_j}}{\partial x_i} - \frac{2}{3}\delta_{ij}\frac{\partial \overline{u_l}}{\partial x_l}\right)\right] \\ -\frac{\partial \overline{p}}{\partial x_i} + \frac{\partial}{\partial x_j}(-\rho \overline{u_i' u_j'}) \end{gathered} \tag{6}$$

In the formula: $\overline{u_i}$ represents the average velocity, m/s; u' represents the fluctuating velocity, m/s; $-\rho \overline{u_i' u_j'}$ represents the Reynolds stress, Pa.

3.2 Hull model

To comprehensively investigate the effectiveness of fairing in reducing ship resistance, this paper selects a container ship under full load as the research object. Under full load, the aerodynamic characteristics of the ship become more complex, which can fully reflect the drag reduction performance of the fairing during actual navigation. The main parameters of the container ship are shown in Table1.

Table 1: Main parameters of container ships

Main parameters	Unit	numerical value
Length overall L	m	196
Beam B	m	32
Ship height H	m	20.1
Container height H_1	m	13
Bridge height H_2	m	15.6
Axial distance between the ship's bow vertex and the foremost containerL_1	m	21.62
Designed draft T	m	12
Designed speed V	kn	20
Wetted surface area S	m^2	42449
Frontal area A_T	m^2	716

In SpaceClaim software, the key structures of container ships (including the hull shell, stacked containers on the deck, and the bridge) are modeled. Due to the structure of large container ships and the stacking of containers on the deck, blind spots are easily formed (Pan, 2006), increasing the risk of navigation accidents. IMO requires that these blind spots be controlled within twice the overall length of the ship. Referring to the design of mainstream ship types with more than 14,000 TEU, the bridge is located about a quarter of the way from the bow and is slightly higher than the containers. After analyzing the limitations of blind spots, it is safe to stack five layers of containers on the deck. The final model is shown in Figure 1.

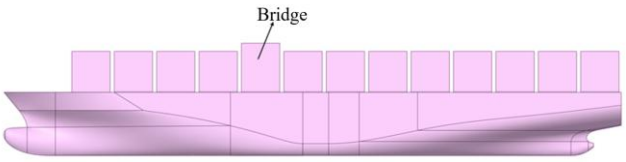

Fig. 1. Ship model

3.3 Computational domain

This article constructs the fluid domain as a rectangular cuboid of sufficient size (Jia et al., 2018), with overall dimensions of 5L × (2L + B) × (2L + H + H2), as shown in Figure 2. The specific construction method is as follows: In the longitudinal direction of the ship, the bow extends forward to the inlet, with a distance of 1 times the ship's length, and the stern extends backward to the outlet, with a distance of 3 times the ship's length; in the transverse direction of the ship, both sides of the hull extend outward to the side boundaries, with a distance of 1 times the ship's length; in the vertical direction of the ship, the hull extends up and down to the upper and lower boundaries, with a distance of 1 times the ship's length.

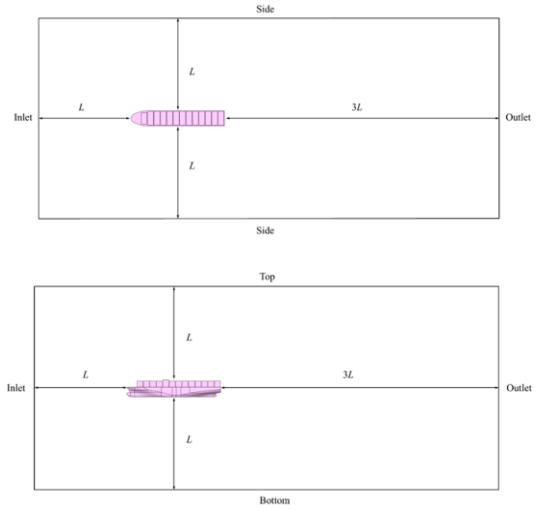

Figure. 2. Fluid domain dimensions

3.4 Mesh generation

In this paper, when analyzing the resistance of container ships, the locally refined grid areas mainly include: the free surface (Xiao et al., 2021), the hull surface, and the near-hull flow field. The locally refined grid areas within the fluid domain are shown in Figure 3.

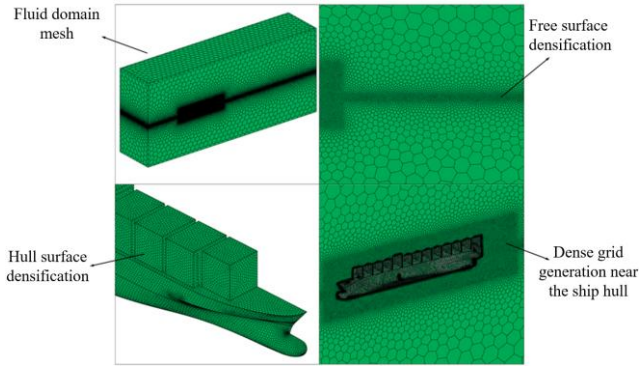

Fig. 3. Mesh generation and mesh refinement

3.5 Solution settings

To accurately simulate the characteristics of ship flow fields, the selection and setting of the solver and computational model in this paper are as follows:

Firstly, considering the fluid as incompressible, a pressure-based unsteady solver suitable for low speeds is selected. Through the two-step process of "solving the velocity field — correcting the pressure equation", the conservation of mass and momentum is satisfied, enhancing the accuracy of the simulation. Secondly, considering the interaction between air and water, the VOF multiphase flow model (Kim et al., 2017) is adopted. By solving the unified momentum equation and tracking the fluid volume fraction, the dynamic behaviours of the medium interface is characterized. Finally, to ensure the physical consistency of the simulation results, a standard atmospheric pressure reference pressure of 101325 Pa is applied to the area above the water surface. The gravity option is enabled, and the vertical acceleration due to gravity is defined.

3.6 Grid-independence verification

To ensure the accuracy of the calculation results, this paper selects the widely used KCS standard ship model data (Wang et al., 2020) in the international shipbuilding field for grid convergence verification. The KCS standard ship model is widely recognized for its rich experimental data and can serve as a reliable reference benchmark. At the 2010 Gothenburg Numerical Ship Hydrodynamics Symposium, researchers provided a series of experimental data for the KCS standard ship model with a rudder. This paper selects the condition with a Froude number F_n=0.2599 for verification, with specific parameters shown in Table 2.

Table 2: Experimental data of KCS standard ship model

Main parameters	Unit	numerical value
Ship length L	m	7.7
Ship speed v	m/s	2.196
Total ship resistance F_T	N	41.869
Total resistance coefficient of ship C_T	N	3.71×10^{-3}
Scaling area of hull and rudder A	m^2	9.55275

Validation of regional grids: Based on the dimensions of the ship model, the minimum grid size in the fluid domain is set to 0.005m in this paper to ensure the quality of the grid for small-scale structures within the fluid domain. The validation data is presented in Table 3..

Table 3: Convergence verification results of each regional grid

Encrypted area	Mesh size (m)	Number of meshes ($\times10^4$)	C_T ($\times10^{-3}$)	Test value ($\times10^{-3}$)	Error (%)
Free surface	0.13	64	4.62	3.71	24.53
	0.064	120	3.94		6.20
	0.057	**246**	**3.66**		**1.35**
	0.033	327	3.66		1.35
Hull surface	0.06	213	3.77	3.71	1.62
	0.05	214	3.75		1.35
	0.04	**217**	**3.66**		**1.07**
	0.03	224	3.66		1.07
hull near-flow field grid	0.08	216	3.66	3.71	1.35
	0.07	217	3.66		1.35
	0.06	**231**	**3.68**		**0.81**
	0.05	235	3.68		0.81

After verifying the grid convergence of three densified grid areas, the final grid sizes selected for each area are: 0.057m for the free surface area, 0.04m for the hull surface, and 0.06m for the near-hull flow field area. Using these grid sizes, the calculation error of the resistance of the KCS ship model can be reduced to 0.81%. Next, these grid sizes will be applied to the container ship studied in this paper. To further ensure consistency with the KCS verification results, in subsequent calculations, we will scale the selected container ship model to the same scale as the KCS ship model to ensure the reliability and accuracy of the verification results.

3.7 Numerical result verification of different turbulence models

In the field of ship resistance calculation, the standard k-ε model, RNG k-ε model, Realizable k-ε model, and SST k-ω model have all demonstrated excellent performance with high accuracy (Liu et al., 2025; Rodrigues et al., 2026; Seok & Park, 2020). To further reduce errors and ensure the reliability of the calculation results, this paper compares and validates the aforementioned turbulence models on the basis of the completed KCS ship model verification, aiming to select the optimal turbulence model most suitable for the research problem at hand. The validation results are presented in Table 4.

Table 4: Turbulence model validation results

Turbulence model	C_T（×10^{-3}）	Test value（×10^{-3}）	Error（%）
Standard *k*-ε model	3.78	3.71	1.89
RNG k-ε model	3.68		0.81
Realizable *k*-ε model	3.69		0.54
SST *k*-ω model	3.77		1.62

It can be observed that, under the premise of verified grid size, the calculation errors of these four turbulence models are not significantly different. Among them, the Realizable k-ε model (Cai et al., 2013) has the highest degree of fit with the research method used in this paper. Therefore, after verification and comparison, the Realizable k-ε model is selected as the turbulence model used in this paper.

Relying on the verified numerical method, we will focus on the drag reduction calculation and flow field analysis of the fairing under level 8 wind.

4. Resistance calculation and analysis

4.1 Selection of calculation speed

Wind force is a vector quantity, consisting of natural wind (determined by weather, with variable intensity and direction, expressed in wind scale) and ship wind (related to ship speed, with direction opposite to ship movement). The vector superposition of the two forms the absolute wind that affects the actual navigation of ships (Huang, 2012), which is a key parameter for analysing ship wind resistance. A level 8 wind on the sea is an extreme wind condition that threatens ship stability, hull strength, cargo, and navigation safety, requiring speed reduction or route avoidance. In this paper, when studying the drag reduction performance of a fairing, level 8 wind speed is taken as the core operating condition; because Fluent calculations use a relative coordinate system (with the hull stationary/flow field moving), the inlet boundary condition needs to be defined as the relative wind speed in the hull coordinate system (the incoming wind speed in the table is the relative wind speed when facing the wind head-on). After scaling, the incoming wind speed is converted using the Froude number similarity criterion to ensure dynamic similarity between the model and the actual ship. The specific calculation of wind speed is shown in Table 5.

Table 5: Calculated wind speed (m/s)

Scale	Wind speed	Select speed	Ship speed	Synthetic wind speed	Scaled wind speed
8	17.2~20.7	20.7	10.3	31.0	6.2

4.2 Numerical calculation results

Since the fairing is only installed above the water surface, its main function lies in guiding airflow and reducing the impact of air resistance on the hull. Currently, when evaluating the drag reduction effect of the fairing, most scholars mainly focus on the analysis of the hull part above the water surface to simplify complex fluid mechanics calculations. Ultimately, without the fairing, the computational domain grid of the ship contains 2,858,533 elements, while with the polygonal curved fairing, the computational domain grid contains 2,886,868 elements. At a wind speed of level 8, the drag of the ship and the drag reduction effect of the fairing are shown in Table 6.

Table 6: Wind resistance results for the ship with polygonal arcuate fairing at 8 beaufort

Fairing type	Drag coefficient /（×10^{-1}）	drag reduction effect（%）
Without a fairing	5.185	-
The polygonal fairing	3.115	39.91

Without a fairing, the wind resistance coefficient of the ship is 0.5185; with a polygonal curved fairing, the wind resistance coefficient of the ship decreases to 0.3115, achieving a drag reduction effect of 39.91%.

4.3 Numerical flow field analysis

4.3.1 Velocity contour

Figure 4 depicts the velocity distribution along the mid-longitudinal section of a ship with and without a polygonal curved fairing under a wind speed of level 8, aiming to investigate the impact of the polygonal curved fairing on the flow field around the hull. Figure 5 illustrates the locations of two velocity monitoring lines, one located at the gap between the ship's bow apex and the first row of containers at x=0.44m, and the other located at the gap between the first and second rows of containers at x=1.37m. Between these two locations, the influence of the fairing on the velocity distribution of the flow field is more significant. Figure 6 presents a line chart based on the relationship between height and velocity, plotting 30 data points from the two monitoring lines. From the above velocity charts, it can be concluded that:

(1) After installing the polygonal curved surface fairing, compared to the condition without a fairing, the high-speed area in front of the fairing is significantly reduced, and the distribution range of high-speed flow is more concentrated. The polygonal curved surface fairing guides the flow field ahead, causing the fluid velocity to gradually slow down in the area near the fairing, thus effectively smoothing the velocity distribution in the bow area and avoiding excessive velocity variations.

(2) After installing the fairing, the velocity gradient around the hull becomes more uniform, exhibiting a smaller overall velocity transition amplitude. Especially in the midship section of the hull, the water flow forms a more closely adhering velocity layer along the hull direction. Without the fairing, the velocity distribution shows greater dispersion, indicating that the fairing can effectively improve the fluid motion characteristics around the hull.

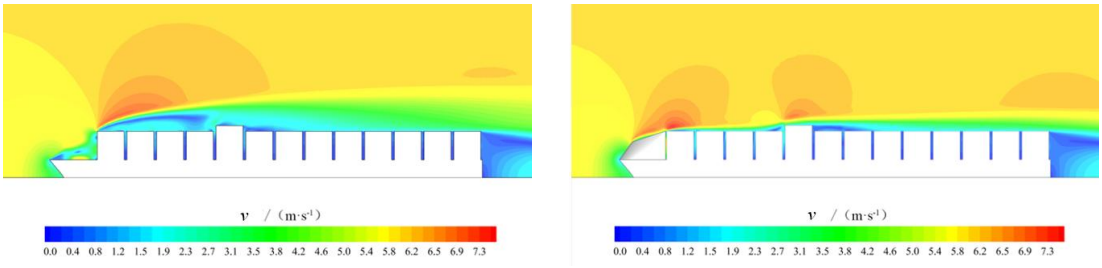

（a）Without a fairing （b）With the polygonal fairing

Figure. 4. Velocity distribution map of longitudinal section in ships

Figure. 5. Monitoring line position for the ship with polygonal arcuate fairing

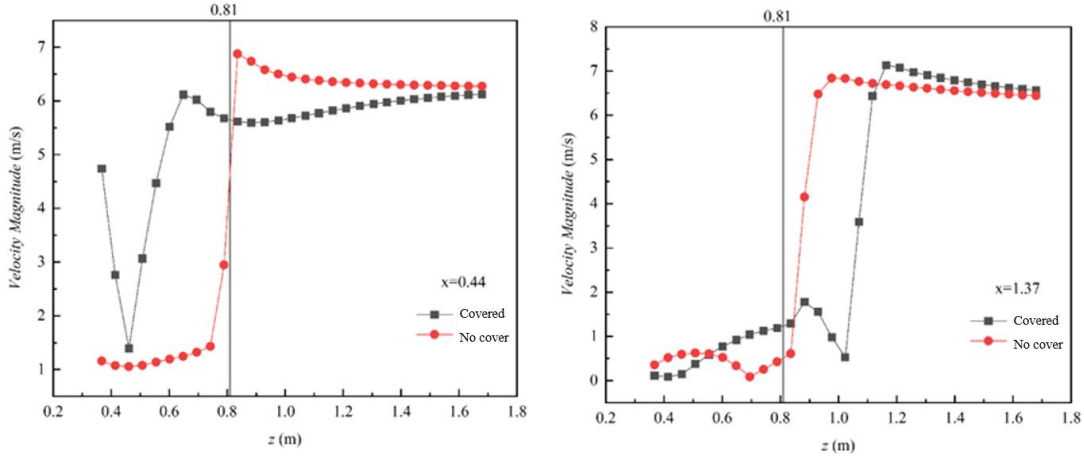

（a）Speed line chart of monitoring line 1 （b）Speed line chart of monitoring line 2

Figure. 6. Velocity profile along the monitoring line for the ship with polygonal arcuate fairing

4.3.2 Streamline diagram

Figure 7 depicts the local velocity streamline diagrams of the front and middle sections of the ship without a fairing and with a polygonal curved fairing, illustrating

the direction of fluid flow and observing whether there are flow vortices, velocity distribution, and changes in flow gradient in the calculation area. The streamline diagram reveals that:

(1) Without a fairing, the airflow in the front and middle of the ship exhibits characteristics of bending and separation, resulting in a relatively chaotic overall flow, especially in front of and above the containers. When the airflow passes through the ship's bow, the fluid in the main flow zone, due to viscous effects, carries away the air close to the ship's surface. This leads to a lack of timely replenishment of air in this area, resulting in a decrease in local pressure. Due to the uneven distribution of pressure, the airflow is pressed towards the wall, forming a body-fitted flow. Due to the viscous effect of the wall, the flow velocity close to the wall gradually slows down.

When body-fitted flow encounters large geometric obstacles, such as the front row of containers at the ship's bow, the streamline bends, and the airflow spreads outwards. Some airflow flows back, forming vortices at the ship's bow and the front of the containers. Some airflow passes over the containers, and under the influence of viscous forces and the pressure difference of deceleration and diffusion, the airflow velocity stops or even reverses, forming vortices and leading to flow separation. It can be observed that after the airflow passes over the front row of containers, the flow separation phenomenon becomes evident. Around the containers, especially above them, a large vortex region is formed. The flow velocity in these vortex regions is low and the direction is unstable, greatly exacerbating the irregularity and turbulence of the airflow. After installing a polygonal curved surface fairing,

(2) After installing the fairing, the streamline distribution in front of the fairing becomes smoother. The fluid is guided by the fairing as it approaches the bow, exhibiting a distinct characteristic of smooth transition. After flowing along the edge of the fairing, the fluid's velocity direction undergoes a slight deflection, but the overall flow direction remains stable. The streamlines in the midship section of the hull are close to the hull surface and exhibit a continuous and smooth distribution characteristic, indicating that the fairing effectively guides the fluid at the front, ensuring it flows smoothly along the hull direction.

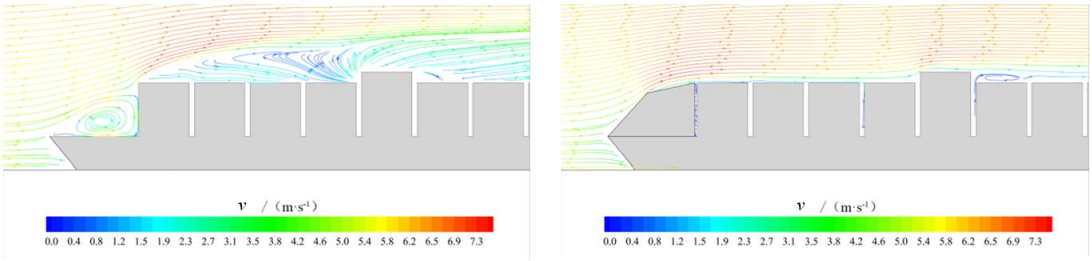

（a）Without a fairing （b）With the polygonal fairing

Figure. 7. Velocity profile along the monitoring line for the ship with polygonal arcuate fairing

4.3.3 Pressure contour plot

Figure 8 shows the pressure contour map on the hull surface under a wind speed of level 8, intuitively reflecting the pressure magnitude and distribution at various locations on the hull through color gradients. Figure 9 is the pressure contour map of the ship's midship section, presenting the pressure distribution of the hull and surrounding fluid from a longitudinal perspective, corresponding to the velocity contour map and streamline diagram of the ship's midship section analyzed earlier. Figure 10 is a pressure coefficient curve diagram of the hull at y=0, depicting the trend of pressure changes on the hull surface. From the above pressure diagrams, we can conclude that:

(1) Without a fairing, a significant pressure gradient is formed due to the pressure difference between the front and rear of the hull, resulting in the generation of pressure drag. It can be observed that regardless of whether a fairing is added, there is always a high-pressure area at the bow and in front of it. This is because the airflow is significantly slowed down by the obstruction of the windward structure, accumulating on the windward side to form a large static pressure. After the high-pressure area, multiple low-pressure areas appear up to the stern. According to the analysis in the previous section, when the airflow bypasses the hull, due to the geometric shape of the hull or sudden changes in flow velocity, the fluid separates from the hull surface. After separation, the fluid forms a reverse backflow, and the kinetic energy of the fluid in the vortex region exists in the form of rotation, with locally high flow velocity.

According to the principle of energy conservation, the total energy of the fluid remains relatively constant, but the increase in kinetic energy is accompanied by a significant decrease in static pressure, thus forming a low-pressure area in the vortex region. Ultimately, the significant difference between the high pressure in front of the hull and the low pressure behind it leads to the generation of pressure drag.

(2) After installing the polygonal fairing, the pressure distribution in the bow area becomes more uniform, with concentrated high-pressure areas of smaller scope. From the longitudinal section pressure contour plot, it can be seen that the fairing effectively diverts the flow at the bow position, resulting in a relatively stable pressure distribution at the bow and reducing the strong pressure difference caused by fluid impacting the bow.

After installing the fairing, the pressure distribution at the midship section of the hull becomes more uniform under the guidance of the fairing. From the pressure coefficient curve, it can be seen that the pressure fluctuation amplitude at the midship section decreases, indicating that the fairing optimizes the pressure variation characteristics on the hull surface and reduces the pressure difference between the fluid and the hull.

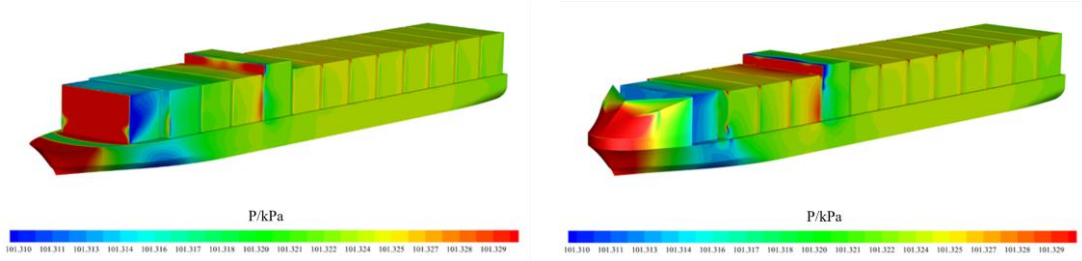

（a）Without a fairing （b）With the polygonal fairing

Figure. 8. Cloud map of ship surface pressure

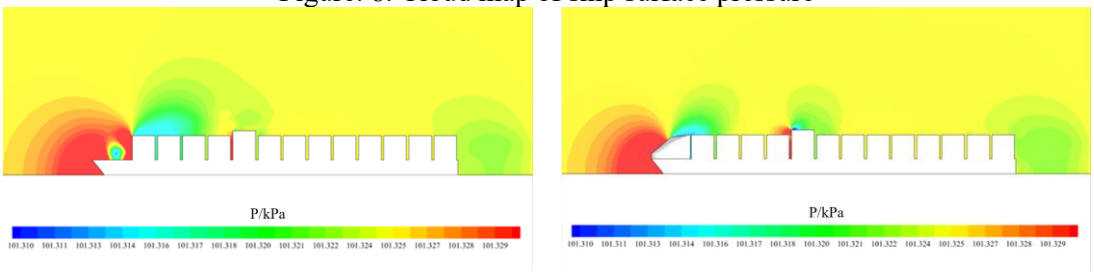

（a）Without a fairing （b）With the polygonal fairing

Figure. 9. Cloud map of longitudinal profile pressure in ships

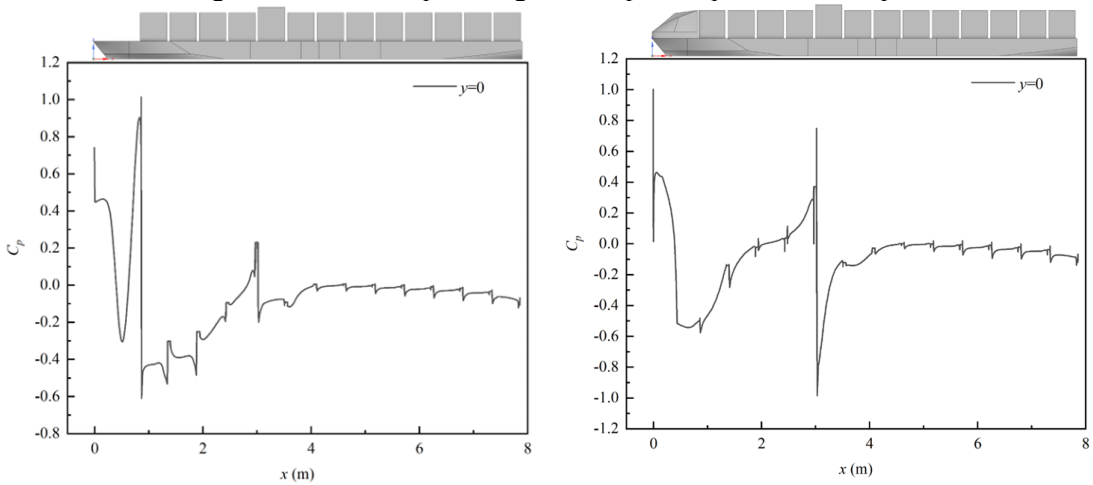

（a）Without a fairing （b）With the polygonal fairing

Figure. 10. Curve of pressure coefficient on the surface of the ship at y=0

5. Conclusion

Based on the CFD numerical simulation method, this article systematically studies the drag reduction performance of polygonal curved surface fairing for large container ships under level 8 wind conditions, with the main conclusions as follows:

The numerical calculation scheme is reliable: verified by the KCS ship model, the grid sizes for the free surface, hull surface, and near-flow field were determined to be 0.057 m, 0.04 m, and 0.06 m, respectively, with a total drag coefficient calculation error of only 0.81%. By selecting the Realizable k-ε turbulence model and VOF multiphase flow model, combined with a pressure-based unsteady solver, the drag characteristics of ships in gas-liquid two-phase flows can be accurately simulated.

The drag reduction effect of the fairing is remarkable: under level 8 wind conditions, after installing the polygonal curved surface fairing, the wind resistance coefficient of the ship decreases from 0.5185 to 0.3115, with a drag reduction rate of 39.91%. This indicates that the fairing can effectively reduce the air resistance of the ship under extreme wind conditions.

The mechanism for flow field improvement is clear: the fairing guides the airflow at the bow, reduces the high-speed area, and mitigates sudden speed changes; optimizes the streamline distribution, inhibits vortex generation, and enables the airflow to flow smoothly along the hull; simultaneously, it equalizes the pressure on the hull surface and reduces pressure drag, thus achieving drag reduction from the perspective of flow field regulation.

Possessing engineering application value: The research results can provide data support for the design and optimization of similar ship fairing designs. The revealed drag reduction logic of "flow guidance - flow stabilization - pressure reduction" also points out the direction for subsequent structural improvements. It can be further extended to different wind levels and speed conditions, and combined with experimental verification to further enhance engineering practicality.

In summary, the polygonal cambered fairing has a significant drag reduction effect on container ships under level 8 wind conditions. The research methods and conclusions are of reference significance for the engineering application and optimization of ship energy-saving technologies.

References

Wang, Z., et al. (2026), Study on total resistance of ships navigating in shallow water, Ocean Engineering, 343, 123463.

Sanz, D. S., et al. (2026), CFD analysis of the influence of biofouling growth on ship resistance under variable trim and draft conditions, Ocean Engineering, 343, 123485.

He, J. Y. (2020), Study on Optimization Method of Ship Resistance Performance Based on RANS Method and SBD Technology [PhD dissertation, Dalian University of Technology].

Grlj, C. G., et al. (2023), The effect of loading conditions and ship speed on the wind and air resistance of a containership, Ocean Engineering, 273, 113991.

Forrest, J. S., Owen, I. (2010), An investigation of ship air wakes using detached-eddy simulation, Computers & Fluids, 39, 656-673.

Viola, I. M. (2009), Downwind sail aerodynamics: A CFD investigation with high grid resolution, Ocean Engineering, 36(12), 974-984.

Wu, B. L., Song, Y. M., Zhang, H. Y., Wang, Y. M., Gu, J. Y. (2025), Research on wind load characteristics and shielding effect of container ship, Journal of Naval University of Engineering, 37(4), 36-44.

Pan, Y. B. (2006), Calculation method of visual blind area for container ships, Containerization, (9), 27-28.

Jia, B. Z., Wu, L. Z., Ji, R., et al. (2018), Prediction and comparison of wind loads on VLCC based on CFD, Journal of Dalian Maritime University, 44(4), 1-7.

Xiao, G., Tong, C., Wang, Y., et al. (2021), CFD simulation of the safety of unmanned ship berthing under the influence of various factors, Applied Sciences, 11(15), 7102.

Kim, M., Hizir, O., Turan, O., et al. (2017), Estimation of added resistance and ship speed loss in a seaway, Ocean Engineering, 141, 465-476.

Wang, Y. D., Chen, Y. Z., Zhou, W. J., et al. (2020), Research on numerical prediction of hull resistance and viscous flow field calculation, Ship Science and Technology, 42(1), 17-22.

Rodrigues, M. I. P., et al. (2026), Uncertainty analysis of a CFD solver for predicting ship motions in head waves, Ocean Engineering, 343, 123129.

Liu, J., et al. (2025), Minimum resistance hull optimization research based on simulation-based design optimization method, Structural and Multidisciplinary Optimization, 68(7), 134.

Seok, J., Park, J. C. (2020), Comparative study of air resistance with and without a superstructure on a container ship using numerical simulation, Journal of Marine Science and Engineering, 8(4), 267.

Cai, W. S., Dong, G. X., Yang, C. Q. (2013), Wind Resistance Simulation of Oil Tankers and Superstructure Optimization in Terms of Wind Resistance, Journal of Shanghai Ship and

Shipping Research Institute, 36(2), 5-10.

Huang, Y. (2012), Research on the model and application of inland waterway ship domain under wind and current action [Doctoral dissertation, Wuhan University of Technology]. Wuhan, China.

Far East Freight Conference's website: www.fareast freightconference.com, last accessed in September 2008.

Received **12 December 2025**

1st Revised **25 December 2025**

Accepted **05 January 2026**